ADVANCED MATERIALS
www.advmat.de

Nanostructuring Multilayer Hyperbolic Metamaterials for Ultrafast and Bright Green InGaN Quantum Wells

*Dylan Lu, Haoliang Qian, Kangwei Wang, Hao Shen, Feifei Wei, Yunfeng Jiang, Eric E. Fullerton, Paul K. L. Yu, and Zhaowei Liu**

Semiconductor quantum well (QW) light-emitting diodes (LEDs) have limited temporal modulation bandwidth of a few hundred MHz due to the long carrier recombination lifetime. Material doping and structure engineering typically leads to incremental change in the carrier recombination rate, whereas the plasmonic-based Purcell effect enables dramatic improvement for modulation frequency beyond the GHz limit. By stacking Ag-Si multilayers, the resulting hyperbolic metamaterials (HMMs) have shown tunability in the plasmonic density of states for enhancing light emission at various wavelengths. Here, nanopatterned Ag-Si multilayer HMMs are utilized for enhancing spontaneous carrier recombination rates in InGaN/GaN QWs. An enhancement of close to 160-fold is achieved in the spontaneous recombination rate across a broadband of working wavelengths accompanied by over tenfold enhancement in the QW peak emission intensity, thanks to the outcoupling of dominating HMM modes. The integration of nanopatterned HMMs with InGaN QWs will lead to ultrafast and bright QW LEDs with a 3 dB modulation bandwidth beyond 100 GHz for applications in high-speed optoelectronic devices, optical wireless communications, and light-fidelity networks.

Since the first demonstration decades ago, semiconductor-based light-emitting diodes (LEDs) have shown superiority in low energy consumption and environmental friendliness for new light source, optical communication, and display.[1,2] With the introduction of III-nitride compound semiconductors,[3] quantum well (QW)-based LEDs nowadays cover various emission wavelengths from UV to infrared.[4] Despite these advances, it has not completely fulfilled its promise as an energy-saving alternative due to its relatively low quantum efficiency especially in the green wavelength region.[5] Besides, the intrinsic long carrier recombination lifetime in the QW heterostructures has also limited the modulation bandwidth of LEDs to a few hundred MHz, which can barely meet today's rapidly increasing requirement for high-speed data transmission.[2,6] In order to improve the performance of QW LEDs, significant effort has been made to enhance the spontaneous carrier recombination rate in III-nitride QWs and their radiative efficiency by material doping and lattice structure engineering yet resulted in a low rate enhancement and a modulation bandwidth below the GHz range.[7,8] Higher dopant concentration in the active region generally leads to severe reduction in the quantum efficiency.[7]

To achieve modulation frequency beyond GHz, the Purcell effect has been increasingly utilized through the interaction between QW emitters and their local electromagnetic environment.[9] By resonantly coupling to surface plasmons, spontaneous emission from III-nitride QWs is strongly modified in the vicinity of plasmonic nanostructures due to local electric-field enhancement.[10] However, since limited metals are available in nature, misalignment of the emission wavelengths with plasmonic resonances results in low enhancement, giving rise to a few narrow bands of working frequencies.[11] This limitation in plasmonic materials has recently been overcome by the emergence of metamaterials, which exhibit designable material properties for imaging and device applications.[12] By realizing hyperbolic dispersion relation, hyperbolic metamaterials (HMMs) made of alternating multilayers have shown the tunability in plasmonic density of states[13] and have already been utilized for significantly advancing molecular emitters.[14–16] Assisted by the nanostructure outcoupling of dominating HMM plasmonic modes, both spontaneous emission rate and far-field radiative intensity in molecules have been improved.[15–17]

In this work, we experimentally demonstrate the ultrafast InGaN/GaN QWs with strongly enhanced emission intensity at the green emission wavelength region by utilizing broadband Purcell enhancement in nanopatterned Ag-Si multilayer HMMs. With well-designed volumetric filling ratio of compositions, Ag-Si multilayer HMMs align the dominating HMM plasmonic modes with the QW emission at green wavelength which significantly enhances the QW recombination rate

Dr. D. Lu, H. Qian, K. Wang, Dr. H. Shen, Dr. F. Wei, Y. Jiang, Prof. E. E. Fullerton, Prof. P. K. L. Yu, Prof. Z. Liu
Department of Electrical and Computer Engineering
University of California
San Diego, 9500 Gilman Drive, La Jolla, CA 92093-0407, USA
E-mail: zhaowei@ucsd.edu
Prof. E. E. Fullerton, Prof. Z. Liu
Center for Memory and Recording Research
University of California
San Diego, 9500 Gilman Drive, La Jolla, CA 92093-0401, USA
Prof. P. K. L. Yu, Prof. Z. Liu
Materials Science and Engineering
University of California
San Diego, 9500 Gilman Drive, La Jolla, CA 92093-0418, USA
The ORCID identification number(s) for the author(s) of this article can be found under https://doi.org/10.1002/adma.201706411.

DOI: 10.1002/adma.201706411

through the Purcell effect. Nanostructuring HMMs outcouples the high-wavevector HMM modes to the far field for improved emission intensity. A close to 160-fold spontaneous emission rate enhancement has been achieved on the nanopatterned HMM-enhanced InGaN QWs across a broadband working wavelength corresponding to a 3 dB modulation speed of about 10.6 GHz. Simultaneously, over tenfold enhancement in QW peak emission intensity was obtained by the nanopatterned HMM. An ultrafast and bright QW LED with a 3 dB modulation bandwidth beyond 100 GHz will be potentially achievable by integrating QWs with such nanopatterned HMMs, leading to new applications in high-speed optoelectronic devices, optical wireless communications, and light-fidelity (Li-Fi) networks.

Figure 1 shows the schematic configuration of QW-based LED enhanced by placing a 2D nanopatterned Ag-Si multilayer HMMs close to the vicinity of the QW emitting layers. The QW LED was grown on a double-side polished sapphire substrate (see the Experimental Section and Figure S1, Supporting Information). As indicated by the bright-field transmission electron microscopy (TEM) image, the active emitting layer consists of three InGaN/GaN QWs with a total thickness of about 30 nm (Figure 1c,d). Optical photoluminescence measurement on the as-grown QW LEDs identifies a QW emission at the green wavelength of 520 nm with a bandwidth of about 36 nm (see the Experimental Section and Figure S2, Supporting Information). Multilayer HMMs made of alternating layers of Ag and Si were sputtered onto the top surface of QWs with well-controlled thickness and volumetric filling ratio before nanopatterns were inscribed into the HMMs by focused ion beam (FIB) milling (see the Experimental Section). A spacer distance of about 8 nm was kept between the plasmonic structures and the first layer of QWs. TEM images show one HMM with a thickness period of about 15 nm and Ag ratio ≈83%. Different ratios were also fabricated with tunable working wavelength as confirmed by the transmission measurement (see Figure S3, Supporting Information). Higher Ag ratio results in blueshift in the plasmonic enhancement wavelength as well as less transmission through the multilayer HMMs. A square lattice was milled into the multilayer HMMs forming

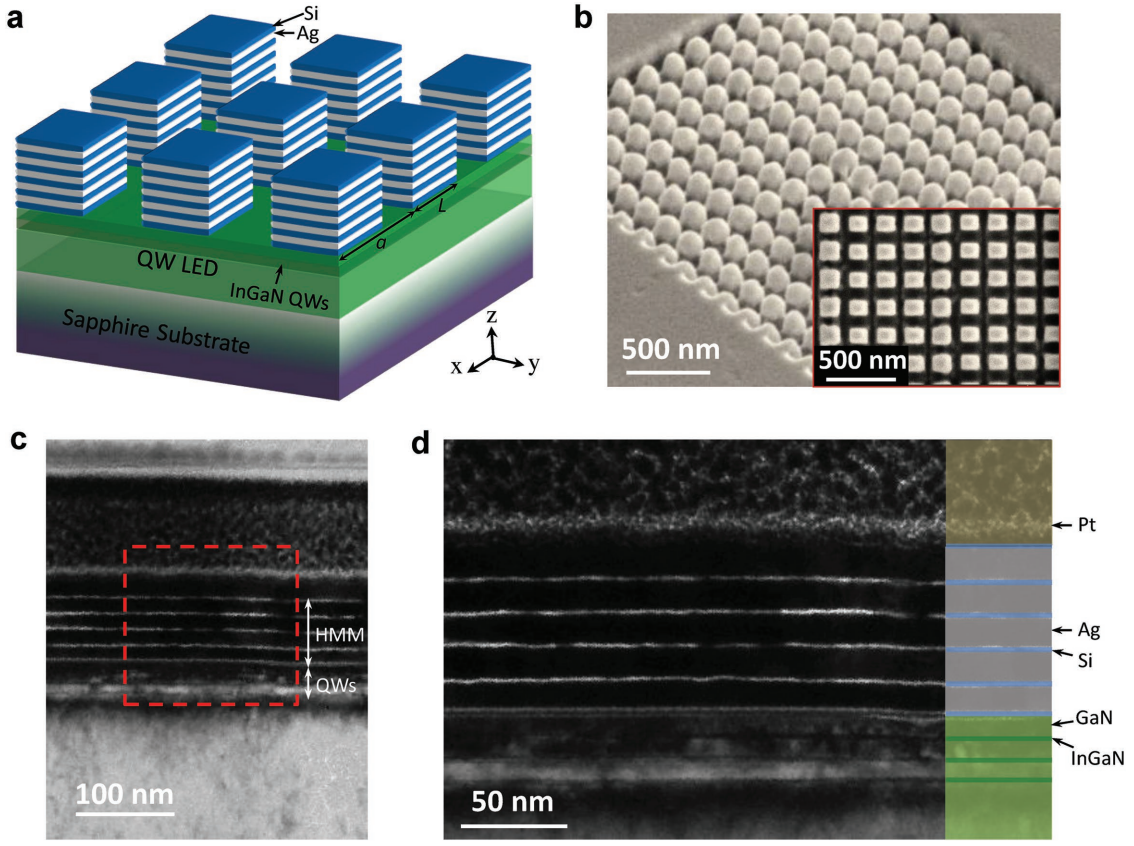

Figure 1. Nanopatterned multilayer HMM enhanced InGaN QWs: a) Schematic configuration of a 2D nanopatterned Ag-Si multilayer HMM on top of an InGaN QW LED. The multilayers consist of Ag-Si stacks with a thickness period of 15 nm and five periods in total in addition to the capping 5 nm Si layer. The volumetric filling ratio of Ag and Si is calibrated and controlled during the growth process. Nanocube array patterns are formed in the multilayers by FIB milling with a period a and length L. The InGaN QW LED has three pairs of InGaN/GaN QWs with a total thickness of about 30 nm. The top-capping GaN barrier layer (≈8 nm) serves as the spacer. b) Perspective-view SEM image of one of the fabricated nanopatterned HMMs (period $a = 200$ nm; length $L = 120$ nm). Inset: Top-view SEM image of the nanocube arrays. c) Bright-field TEM image of the cross-sections of Ag-Si multilayer HMMs on InGaN QWs, showing well-formed periodic lattice structures. In the HMM, the white color corresponds to Si and the black color corresponds to Ag. d) Zoom-in bright-field TEM image corresponding to the red dashed square in (c) with the color schematics mapping the material composition. The thickness for Ag and Si are ≈12.4 nm and ≈2.6 nm, respectively, forming a ≈83% volumetric filling ratio. The thick Pt forms a protection layer for FIB cross-sectioning and TEM imaging.

2D HMM nanocube arrays with a spatial period of 200 nm right on the QWs as shown in the scanning electron microscopy (SEM) image in Figure 1b.

The strong interaction between QW emission and nearby nanopatterned HMMs is enabled as the emission wavelength approaches the plasmonic resonance of the HMMs. Large plasmonic density of states in HMMs induces dramatic Purcell enhancement in the QW light emission process. To understand such interaction, a theoretical calculation of the Purcell factor based on the modified theory of dipole interaction with metallic substrates was carried out for the QW system by modeling the spontaneous emission from QWs as individual dipoles (see Section S1, Supporting Information).[18] **Figure 2**a–c shows the Purcell interaction of a QW dipole emitter with a uniform Ag-Si multilayer HMM separated at a distance d along z-axis. The multilayer HMMs consist of 11 alternating layers of Ag and Si with a thickness period of 15 nm and the bottom Si layer near the QW emitters. Compared to the fixed Purcell enhancement at 440 nm using pure Ag, multilayer HMMs shift to longer wavelengths by gradually decreasing the Ag volumetric filling ratio, which agree well with the characterization of fabricated multilayer HMMs (see Figure S3, Supporting Information). A 83% of Ag in the HMMs was selected for the InGaN/GaN QWs as the resulting Purcell enhancement aligns with the green QW emission wavelengths. Such Purcell interaction also strongly depends on the distance d between the QW emitters and the HMMs. Figure 2c indicates the dramatically increased Purcell factor from ninefold to about 170-fold as QW emitters approaches the HMM from 25 to 8 nm. Corresponding radiative enhancement stays moderate and decreases slightly near the peak Purcell enhancement at 527 nm. A complete study of Purcell interaction dependence on d further confirms the exponential decay of the Purcell factor at $d < 30$ nm before converging to negligible plasmonic interaction, whereas the radiative enhancement is periodically oscillating in front of the HMM surface with a maximum of 3.5-fold enhancement which reflects the wave interference nature of the Purcell effect (see Figure S4, Supporting Information).

The moderate radiative enhancement near the uniform multilayer HMMs can be improved by outcoupling the HMM plasmonic modes.[15] An outcoupling nanopattern with a square lattice of period a and HMM nanocube size L was designed into the uniform multilayer HMMs near the QW emitters (Figure 2d). The plasmonic modes supported by the uniform HMM typically have wavevectors much larger than that of free-space photons, which prevents the propagation of such modes into the far field. The lattice wavevectors of the HMM nanocube array compensate such wavevector mismatch, resulting in efficient outcoupling of the plasmonic modes to radiative photons.

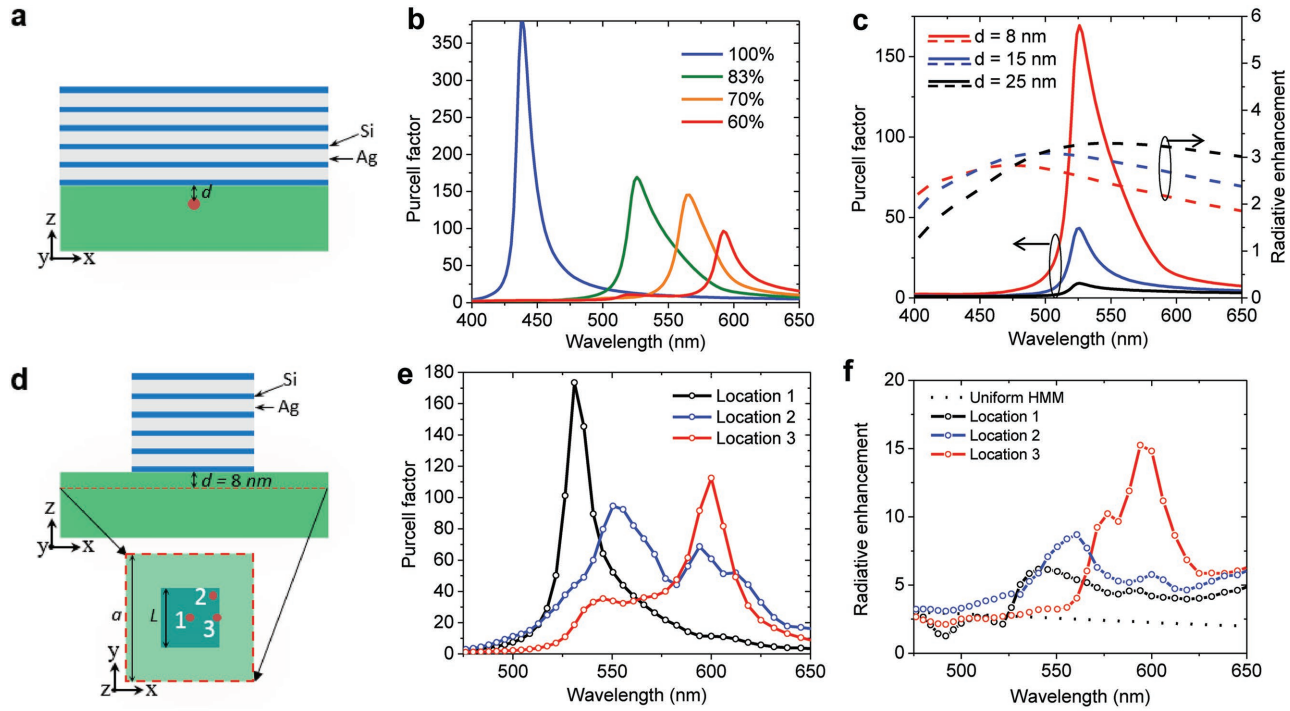

Figure 2. Theoretical study of Purcell enhancement of InGaN QWs by uniform and nanopatterned multilayer HMMs: a) Schematics of a uniform Ag-Si multilayer HMM on top of an InGaN QW substrate with a QW dipole emitter separated a distance of d from the HMM along z-axis. The multilayers consist of five pairs of Ag-Si stacks with a thickness period of 15 nm plus a capping 5 nm Si layer. b) Tunable Purcell factor for an isotropically polarized QW dipole emitter located $d = 8$ nm below the uniform Ag-Si multilayer HMM with different volumetric filling ratios of Ag and Si. The label provides the filling ratios of Ag. c) Purcell factor (solid lines) and radiative enhancement (dashed lines) for an isotropic QW dipole emitter located at different distances below the uniform Ag-Si multilayer HMM with an Ag filling ratio of 83%. d) Schematics of one unit cell of a nanopatterned Ag-Si multilayer HMM on top of an InGaN QW substrate with a QW dipole emitter at a distance of $d = 8$ nm. The nanopatterned HMM has an array period of $a = 200$ nm and length of $L = 100$ nm. Red dashed square shows dipole locations in the x–y plane viewed from the QW side. Coordinates for locations 1, 2, and 3 are $(x, y) = (0$ nm, 0 nm), (40 nm, 40 nm), and (50 nm, 0 nm), respectively. e,f) Purcell factor (e) and radiative enhancement (f) corresponding to the isotropic QW dipoles at locations indicated in (d). Black dashed line corresponds to the uniform HMM case.

The interaction between QW dipole emitters and HMM nanopatterns with different periods was modeled and calculated using 3D full-wave simulation (see Section S1 and Figure S5, Supporting Information). While the Purcell factor keeps relatively constant for different periods, the radiative enhancement dramatically increases for smaller pattern periods and reaches a maximum at 200 nm which provides the best outcoupling efficiency and compatibility with practical fabrication. For a period of 200 nm, the Purcell enhancement was further mapped spatially in the x–y plane at d = 8 nm with peak performance at three locations provided in Figure 2e,f. QW emitters at location 1 have a similar wavelength-dependent Purcell factor to uniform HMMs with a peak enhancement of about 170-fold at the wavelength of 527 nm. However, corresponding radiative enhancement has been improved to sixfold thanks to the outcoupling of HMM plasmonic modes. Supported by different plasmonic modes in the HMM nanocubes, Purcell factors at locations 2 and 3 get redshifted to the 550 and 600 nm wavelengths, respectively, with preserved two orders of magnitude enhancement. Their radiative enhancement has also been increased to more than tenfold. Incorporation of nanopatterns into the HMMs dramatically broadens the working wavelength of Purcell enhancement, resulting in an ultrafast and bright QW across a broad visible wavelength range. These theoretical results only account for the representative interaction of individual QW dipole emitters with the HMMs, whereas in practical samples such interaction includes a collective contribution from dipole emitters in all three QWs at various positions to the HMMs.

The dynamic interaction of InGaN QWs with nanopatterned multilayer HMMs was experimentally characterized by time-resolved photoluminescence in a two-photon microscope (see the Experimental Section and Figure S6, Supporting Information). **Figure 3**a shows the measured time-resolved photoluminescence decay curves (open circles) at the wavelength of 527 nm, with peak counts normalized to unity, corresponding to the green InGaN QWs coated with uniform or nanopatterned Ag-Si multilayer HMMs whose morphology is given in Figure 1. As-grown green InGaN QWs were found to have a lifetime of about 10.2 ns, which fits well with a single exponential decay (solid black line). Compared to the slow single-exponential decay in as-grown QWs, the Purcell interaction with multilayer HMMs dramatically enhances the QW recombination rate which can be interpreted as the collective responses of multi-QWs after a multiexponential decay fitting.[15] For the nanopatterned HMM with a period of 200 nm, the QW photoluminescence decays initially at a fast recombination rate of 1/65 ps^{-1}, which is dominated by the QW closest and strongly coupled to the nanopatterns, before reducing to 1/2.5 ns^{-1} which is mainly contributed by the QW farthest from the HMM.[15] In comparison, carrier recombination for QWs near the uniform HMM was found to have a fast and slow decay at 1/2.2 and 1/2.6 ns^{-1}, respectively. Thanks to the nanopattern outcoupling of high-wavevector plasmonic modes, the nanopatterned HMM can further enhance the QW recombination rate by totally 157-fold as compared with only fivefold for the uniform HMM. Such nanostructure outcoupling not only makes the fast-recombining channel accessible in the far field but also leads to significantly increased photoluminescence peak intensity (see Figure S7, Supporting Information). Instead of merely 2.4-fold peak intensity improvement in the uniform HMM, an about tenfold enhancement in QW peak emission intensity was simultaneously achieved in the nanopatterned HMM. The incorporation of nanopatterned HMMs with InGaN QWs realized an ultrafast plasmonic enhanced QW LEDs for high-speed direct modulation with a maximum 3 dB modulation frequency of about 10.6 GHz, which is greatly improved from the corresponding 68 MHz of an as-grown InGaN QW LED (see Section S2, Supporting Information). High-speed modulation beyond 100 GHz is achievable if combining such nanopatterned HMMs with as-grown QW LEDs that have a modulation bandwidth larger than 700 MHz (see Section S2, Supporting Information).

The spatial dependence of time-resolved photoluminescence of InGaN QWs has been mapped experimentally by scanning the excitation laser spot across the area with uniform and nanopatterned multilayer HMMs (see the Experimental Section). Figure 3b–d shows the spatial mapping of recombination

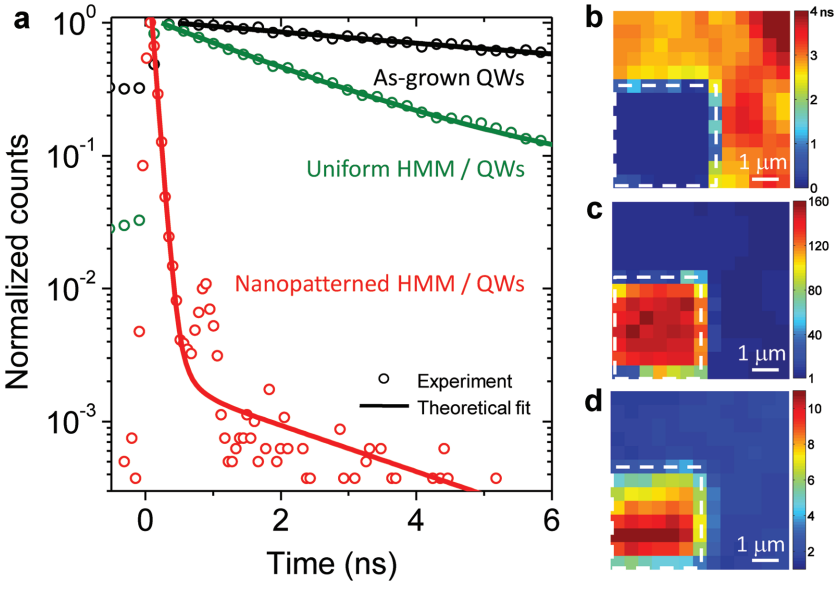

Figure 3. Experimental measurements of time-resolved photoluminescence for InGaN QWs with different sample configurations: a) Time-resolved photoluminescence measurement for as-grown InGaN QWs (black open circles), QWs with uniform Ag-Si multilayer HMMs (green open circles), and with nanopatterned HMMs (red open circles) after being normalized to the maximum of individual curves observed at an emission wavelength of 527 nm with a bandwidth of 16 nm. Nanocube array period, 200 nm. Corresponding theoretical fit curves in solid lines explain well the spontaneous photoluminescence behavior in the time domain. b–d) Spatial mapping of spontaneous recombination lifetime (b), Purcell factor (c), and peak emission intensity enhancement (d) of InGaN QWs with an Ag-Si multilayer HMM at the emission wavelength of 527 nm with a bandwidth of 16 nm. The white dashed square outlines the nanopatterned region. Purcell factor and peak emission intensity enhancement are compared with as-grown InGaN QWs.

lifetime of InGaN QWs near the HMMs and its corresponding Purcell factor and peak emission intensity enhancement at the emission wavelength of 527 nm, where the dashed white line separates the region with a nanopatterned HMM from the rest uniform area. The nanopatterned HMM uniformly enhances the QW recombination rate to about 1/65 ps^{-1} whereas it stays slow near a uniform HMM. The corresponding Purcell factor reaches over two orders of magnitude in the nanopatterned region with over tenfold peak emission intensity enhancement compared to as-grown QWs, yet there are only a small improvement in the uniform HMM region. The nanopatterned HMMs makes the QWs much faster and brighter than the as-grown QWs or those with uniform HMMs.

To better understand the dynamics of the Purcell interaction between InGaN QWs and HMMs, wavelength-dependent time-resolved photoluminescence measurement was carried out with photon emissions selectively recorded over a range of specific wavelengths with the aid of a monochromator (see the Experimental Section). **Figure 4**a–c shows the wavelength scanning for time-resolved photoluminescence across a broad range of about 100 nm for as-grown InGaN QWs and those with uniform and nanopatterned multilayer HMMs. The recombination rate of InGaN QWs was strongly enhanced by the nanopatterned HMM in a broad wavelength range with significantly improved peak emission intensity. A quantitative comparison between these three types of samples is provided in Figure 4d–f with the extracted spectra of lifetime (Figure 4d) and corresponding peak emission intensity (Figure 4e). Unlike the constantly long recombination lifetime near 10 ns for as-grown InGaN QWs, nanopatterned HMMs have dramatically reduced lifetime to <70 ps in a 100 nm wavelength range, which is far more effective than using uniform HMMs whose lifetime is only reduced to a few ns. The Purcell factor obtained from this measurement indicates more than 110-fold recombination rate enhancement by the nanopatterning in the broad wavelength range as compared to less than sevenfold by the uniform HMMs (Figure 4f). Besides, peak emission intensity for the QWs with nanopatterned HMM has also been increased by one to two orders of magnitude in the same detection wavelengths instead of less than threefold enhancement in the uniform HMMs (Figure 4f). Such broadband ultrafast and bright InGaN QWs have been made possible by the multimode plasmonic responses from the nanopatterned multilayer HMMs (see Figure 2).

In summary, we have demonstrated an ultrafast and bright green InGaN QW LED enhanced by nanostructuring Ag-Si multilayer HMMs. The nanopatterned HMMs support strong Purcell enhancement near the QW emission wavelength and outcouple multiple plasmonic modes, resulting in more than two order-of-magnitude enhancement in the QW recombination rate across a broadband of wavelengths with simultaneously more than tenfold emission intensity improvement when compared to only a few times change by HMMs alone. A high-speed 3 dB modulation bandwidth beyond 100 GHz will be possible by integrating such nanopatterned HMMs into

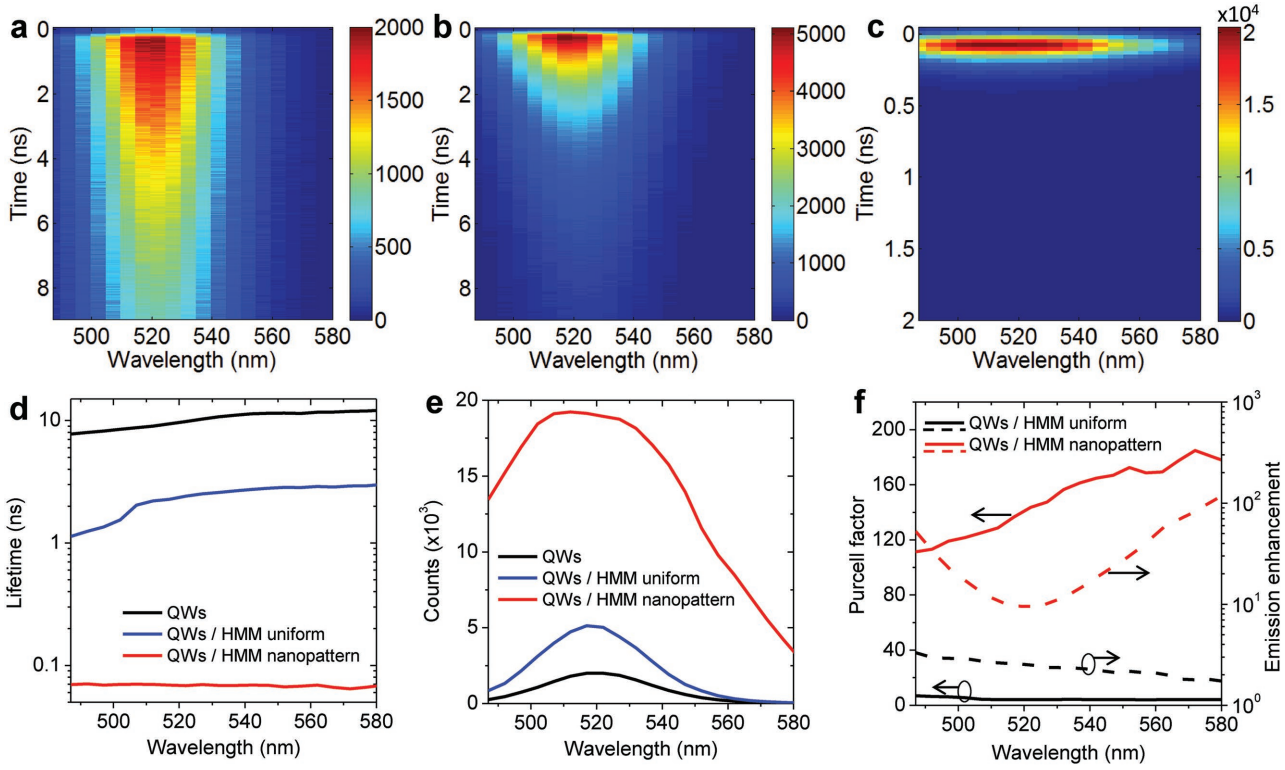

Figure 4. Wavelength-dependent time-resolved photoluminescence for InGaN QWs with different sample configurations: a–c) Wavelength scanning for time-resolved photoluminescence from the wavelength 485 to 580 nm for as-grown InGaN QWs (a), QWs with uniform (b) and nanopatterned Ag-Si multilayer HMMs (c). The intensity corresponds to the photon counts. d,e) Wavelength-dependent recombination lifetime and photon counts at the peak intensity extracted from results in (a)–(c). f) Wavelength spectra of Purcell factor (solid lines) and peak emission enhancement (dashed lines) for QWs with uniform (black lines) and nanopatterned (red lines) Ag-Si multilayer HMMs, as compared with as-grown InGaN QWs.

QW LEDs. Combined with the nanopattern transfer technology with further development in the control of unit cell size,[19] it is promising to scale up the metamaterial-enabled ultrafast LEDs for practical large-area device applications. This type of nanopatterned HMMs can also be applied to LEDs emitting at other wavelengths and with different emitting materials and dimensionality, paving the way for the integration with electrically injected LEDs in the future.

Experimental Section

Growth of InGaN QWs: InGaN/GaN multi-QW LED wafers were grown using a metal organic chemical vapor deposition system (Thomas Swan close-coupled showerhead 3 × 2"). 2-inch double-side polished c-sapphire wafers were used as the substrates. Traditional low-temperature (530 °C) GaN nucleation layer method was used followed by high-temperature (HT, 1040 °C) GaN buffer layer for the material growth.[20] Subsequently a 1.1 µm HT n^+-GaN ($n \approx 5 \times 10^{18}$ cm^{-3}), and three periods of InGaN/GaN multi-QWs were grown. The multi-QWs were grown at temperatures of 675 and 840 °C for InGaN wells (growth thickness 2 nm) and GaN barriers (growth thickness 10 nm), respectively. The top-capping GaN barrier layer serves as the spacer.

Fabrication of Nanopatterned Multilayer HMMs: Ag-Si multilayers, composed of five pairs of Ag and Si layers with a 5 nm thick capping Si layer, were prepared by alternatively d.c. magnetron sputtering Si and Ag layers onto the top surface of InGaN/GaN QW LED substrates at room temperature. Sputtering rates for Ag and Si at 50 W (≈2.5 W cm^{-2}) were 1.6 and 0.3 Å s^{-1}, respectively, as determined by low-angle X-ray reflectivity measurements of calibration sample film thicknesses. The 5 nm capping layer helps prevent Ag oxidation. The base pressure of the chamber was 5×10^{-8} torr and the Ar pressure was fixed at 2.7 mtorr. The period thickness of Ag and Si was fixed at 15 nm with different volumetric ratios controlled by the growth times and sputtering rates. Nanoscale trenches were inscribed into the multilayers by FIB milling to form nanocube arrays.

Measurement of Photoluminescence: Photoluminescence spectra of the InGaN/GaN multi-QW LED samples were measured by a microspectroscopic system. After excited by a 405 nm continuous-wave laser, emission from the QWs was collected with an objective of 50×, numerical aperture (NA) = 0.55 and a long-pass filter (409 nm) before resolved by a Czerny–Turner spectrograph (Andor Shamrock 303i). The spectrograph was equipped with a diffraction grating of 150 lines mm^{-1} and a blaze wavelength at 500 nm, and a charge coupled device (CCD) camera (Andor Newton CCD). A dichroic beamsplitter (405 nm) was also used to block the detection of laser light.

Measurement of Time-Resolved Photoluminescence: The recombination rate and lifetime of the InGaN QWs with various HMM samples were measured by time-resolved photoluminescence in a two-photon microscopy system. A Ti:Sapphire laser system (Spectra-Physics Mai Tai) with a pulse width of less than 100 fs and a repetition rate of 80 MHz was applied to excite the QWs, from the sapphire substrate side of the InGaN QW wafer, at an excitation wavelength of 800 nm. A dichroic short-pass beamsplitter (690 nm) was used to block the laser light from the detection. The photoluminescence signal was collected by a 20× objective with 0.45 numerical aperture and filtered by a series of optical components to improve the signal to noise ratio, including a short-pass filter (690 nm), two BG39 glass windows (<600 nm pass), and a pinhole before entering a monochromator. The monochromator selects the output wavelength across the visible region with a switchable bandwidth before the photos are recorded by a Horiba picosecond photon detection module. A typical collection bandwidth of 16 nm was used for reasonable photon signal. The spatial mapping of time-resolved photoluminescence was enabled by scanning the laser spot across the QW sample using a nanostage controlled by a two-axis electronic controller (Mad City Labs Inc. Nano-Drive 85). A step size of 1 µm was used with a 10 ms delay and 10 s dwell time at each pixel.

Supporting Information

Supporting Information is available from the Wiley Online Library or from the author.

Acknowledgements

The authors acknowledge financial support from National Science Foundation - Division of Materials Research (Grant No. 1610538). The authors thank J. J. Kan, S. Montoya, W. Lu, J. Song, and S. K. Sinha for assistance during various phases of the experiments. Z.L. conceived the concept. D.L. and H.Q. performed numerical modeling and simulations. D.L. grew multilayer HMM and fabricated the HMM nanopatterns. K.W. grew the green InGaN QW LEDs with supervision from P.K.L.Y. H.S., F.W., and D.L. designed and built the time-resolved photoluminescence system with wavelength scanning and spatial mapping. D.L. performed the optical experiments and prepared all the figures. H.Q. prepared the cross-sectional sample for TEM. Y. J. took the TEM images. E.E.F. supervised the thin-film sputtering system. D.L. and Z.L. wrote the paper. All authors discussed the results and contributed to the revision of the paper. Z.L. supervised the project.

Conflict of Interest

The authors declare no conflict of interest.

Keywords

light-emitting diodes, metamaterials, multilayers, plasmonics, Purcell effect

Received: November 3, 2017
Revised: December 28, 2017
Published online:

[1] R. N. Hall, G. E. Fenner, J. D. Kingsley, T. J. Soltys, R. O. Carlson, *Phys. Rev. Lett.* **1962**, *9*, 366.
[2] E. F. Schubert, *Light-Emitting Diodes*, 2nd ed., Cambridge University Press, New York, NY **2006**.
[3] S. Nakamura, T. Mukai, M. Senoh, *Appl. Phys. Lett.* **1994**, *64*, 1687.
[4] S. Pimputkar, J. S. Speck, S. P. DenBaars, S. Nakamura, *Nat. Photonics* **2009**, *3*, 179.
[5] a) E. F. Schubert, J. K. Kim, *Science* **2005**, *308*, 1274; b) A. Khan, *Nat. Photonics* **2009**, *3*, 432.
[6] a) T. P. Lee, T. Li, *Semicond. Semimetals* **1985**, *22*, 281; b) D. C. O'Brien, L. B. Zeng, H. Le-Minh, G. Faulkner, J. W. Walewski, S. Randel, *PIMRC 2008. IEEE 19th Int. Symp. on Personal, Indoor and Mobile Radio Communications*, IEEE, Piscataway, NJ, USA **2008**, http://doi.org/10.1109/PIMRC.2008.4699964.
[7] C. H. Chen, M. Hargis, J. M. Woodall, M. R. Melloch, J. S. Reynolds, E. Yablonovitch, W. Wang, *Appl. Phys. Lett.* **1999**, *74*, 3140.
[8] a) P. Waltereit, O. Brandt, A. Trampert, H. T. Grahn, J. Menniger, M. Ramsteiner, M. Reiche, K. H. Ploog, *Nature* **2000**, *406*, 865; b) J.-W. Shi, H.-Y. Huang, J.-K. Sheu, C.-H. Chen, Y.-S. Wu, W.-C. Lai, *IEEE Photonics Technol. Lett.* **2006**, *18*, 1636; c) J. W. Shi, K. L. Chi, J. M. Wun, J. E. Bowers, Y. H. Shih, J. K. Sheu, *IEEE Electron Device Lett.* **2016**, *37*, 894; d) A. Rashidi, M. Monavarian, A. Aragon, S. Okur, M. Nami, A. Rishinaramangalam, S. Mishkat-Ul-Masabih, D. Feezell, *IEEE Photonics Technol. Lett.* **2017**, *29*, 381.

[9] a) E. M. Purcell, *Phys. Rev.* **1946**, *69*, 681; b) I. Gontijo, M. Boroditsky, E. Yablonovitch, S. Keller, U. K. Mishra, S. P. DenBaars, *Phys. Rev. B* **1999**, *60*, 11564.

[10] a) K. Okamoto, I. Niki, A. Shvartser, Y. Narukawa, T. Mukai, A. Scherer, *Nat. Mater.* **2004**, *3*, 601; b) K. Okamoto, I. Niki, A. Scherer, Y. Narukawa, T. Mukai, Y. Kawakami, *Appl. Phys. Lett.* **2005**, *87*, 071102; c) C. Y. Yang, A. A. Bettiol, Y. Shi, M. Bosman, H. R. Tan, W. P. Goh, J. H. Teng, E. J. Teo, *Adv. Opt. Mater.* **2015**, *3*, 1703; d) M. K. Kwon, J. Y. Kim, B. H. Kim, I. K. Park, C. Y. Cho, C. C. Byeon, S. J. Park, *Adv. Mater.* **2008**, *20*, 1253.

[11] a) D. M. Yeh, C. F. Huang, C. Y. Chen, Y. C. Lu, C. C. Yang, *Nanotechnology* **2008**, *19*, 345201; b) X. F. Gu, T. Qiu, W. J. Zhang, P. K. Chu, *Nanoscale Res. Lett.* **2011**, *6*, 199; c) K. Tateishi, M. Funato, Y. Kawakami, K. Okamoto, K. Tamada, *Appl. Phys. Lett.* **2015**, *106*, 121112; d) S. C. Zhu, Z. G. Yu, L. X. Zhao, J. X. Wang, J. M. Li, *Opt. Express* **2015**, *23*, 13752.

[12] a) Z. Liu, H. Lee, Y. Xiong, C. Sun, X. Zhang, *Science* **2007**, *315*, 1686; b) L. Ferrari, C. H. Wu, D. Lepage, X. Zhang, Z. W. Liu, *Prog. Quantum Electron.* **2015**, *40*, 1; c) S. Jahani, Z. Jacob, *Nat. Nanotechnol.* **2016**, *11*, 23; d) J. Rho, Z. L. Ye, Y. Xiong, X. B. Yin, Z. W. Liu, H. Choi, G. Bartal, X. Zhang, *Nat. Commun.* **2010**, *1*, 143; e) X. J. Ni, Z. J. Wong, M. Mrejen, Y. Wang, X. Zhang, *Science* **2015**, *349*, 1310; f) J. B. Sun, M. I. Shalaev, N. M. Litchinitser, *Nat. Commun.* **2015**, *6*, 7201.

[13] a) D. Lu, Z. Liu, *Nat. Commun.* **2012**, *3*, 1205; b) C. L. Cortes, W. Newman, S. Molesky, Z. Jacob, *J. Opt.* **2012**, *14*, 063001; c) X. Yang, J. Yao, J. Rho, X. Yin, X. Zhang, *Nat. Photonics* **2012**, *6*, 450; d) Y. Cui, K. H. Fung, J. Xu, H. Ma, Y. Jin, S. He, N. X. Fang, *Nano Lett.* **2012**, *12*, 1443; e) A. Poddubny, I. Iorsh, P. Belov, Y. Kivshar, *Nat. Photonics* **2013**, *7*, 948.

[14] a) Z. Jacob, J.-Y. Kim, G. V. Naik, A. Boltasseva, E. E. Narimanov, V. M. Shalaev, *Appl. Phys. B* **2010**, *100*, 215; b) J. Kim, V. P. Drachev, Z. Jacob, G. V. Naik, A. Boltasseva, E. E. Narimanov, V. M. Shalaev, *Opt. Express* **2012**, *20*, 8100.

[15] D. Lu, J. J. Kan, E. E. Fullerton, Z. Liu, *Nat. Nanotechnol.* **2014**, *9*, 48.

[16] K. V. Sreekanth, K. H. Krishna, A. De Luca, G. Strangi, *Sci. Rep.* **2014**, *4*, 06340.

[17] L. Ferrari, D. Lu, D. Lepage, Z. Liu, *Opt. Express* **2014**, *22*, 4301.

[18] G. W. Ford, W. H. Weber, *Phys. Rep.* **1984**, *113*, 195.

[19] D. Chanda, K. Shigeta, S. Gupta, T. Cain, A. Carlson, A. Mihi, A. J. Baca, G. R. Bogart, P. Braun, J. A. Rogers, *Nat. Nanotechnol.* **2011**, *6*, 402.

[20] S. Nakamura, *Jpn. J. Appl. Phys.* **1991**, *30*, L1705.